Kinetics of graphitization of thin diamond-like carbon (DLC) films catalyzed by transition metal

N. Boubiche, J El Hamouchi, J Hulik, M Abdesslam, C Speisser, F Djeffal, Francois Le Normand

Kinetics of graphitization of thin diamond-like carbon (DLC) films catalyzed by transition metal

N. Boubiche[1,2], J. El Hamouchi[1], J. Hulik[1], M. Abdesslam[1,3], C. Speisser[1], F. Djeffal [4] and F. Le Normand[1,*]

1: MaCEPV/ICube, Université de Strasbourg and CNRS, STRASBOURG, 23 rue de Loess, BP 20CR, 67037 STRASBOURG, FRANCE.

2: Department of Physics, University of BATNA-1, 05000 BATNA, ALGERIA.

3: Department of Radiation Physics, University of Science and Technology Houari Boumediene, ALGER, ALGERIA.

4: Department of Electronics, University of BATNA-2, 05000 BATNA, ALGERIA.

** To whom any correspondence should be addressed: Dr F. Le NORMAND, Tel 33 3 88 10 65 46; email : francois.le-normand@unistra.fr*

Highlights

Kinetics of graphitization of diamond like carbon films coated with Ni nanoparticles;

High electrical conductivities of Ni-coated diamond like carbon films;

Raman mapping of graphitic fragments in Ni-coated diamond like carbon films.

Prime Novelty and projected Interest:

Kinetics of graphitization at 773K of thin diamond-like carbon (DLC) films coated with minute amount of Ni metallic particles;

High surface electrical conductivities, which are quite promising and competitive in comparison to literature data dealing with transparent electrodes.

Correlation between conductivity models and Raman measurements in Catalytic metal/DLC material

Keywords: diamond-like carbon; thin graphite films; metal catalyst; pulsed laser deposition, thermal treatment; Raman spectroscopy, optical transmission and absorption; electric transport measurements.

Abstract

In this paper, we have studied the kinetics of graphitization at 773K of thin diamond-like carbon (DLC) films coated with minute amount of Ni metallic particles. DLC films are deposited at room temperature by pulsed laser deposition (PLD) on a transparent quartz substrate, and Ni is deposited on the surface of DLC using molecular beam epitaxy technique at room temperature. The ultra-high vacuum thermal (range 573-873K with 60 min annealing treatments) and kinetic (range 30-3760 min at 773K) behaviors of the deposited films are investigated. Surface and interface characterizations indicate that the growth of graphitic sp^2 clusters starts at temperatures lower than 573K. The kinetics of graphitization is recorded at 773K. Thus, the continuous growth of graphitic clusters leads to a long-range kinetics. These clusters are responsible for the increase in the electrical conductivity and carrier mobility, reaching values of 6.10^3 Siemens/cm and 20 $V/cm^2 \times s$, respectively. This continuous change is not only explained by the nucleation and growth of graphitic clusters, but also by some reorientation of them alongside both the surface and the quartz substrate. The obtained results demonstrate that thermally post-treated catalytic metal/DLC films are promising materials for conductive electrodes and sensing applications.

1. Introduction

Graphene is a 2D planar material of hexagonal structure comparable to a honeycomb network [1]. This unique structure infers outstanding properties like very large electrical [2] and thermal [3] conductivities, a high planar Young modulus combined with a high flexibility [4] and optical transparency [5]. In addition, ultra-thin graphitic films (UTGF) exhibit properties close to those of the graphene monolayer, at least with graphitic layers less than 5 monolayers [6]. However, applications of UTGF as transparent electrodes require new elaboration technique with large size, low-temperature and thickness control. Moreover, it is also recommended to grow UTGF films directly on an appropriate substrate to avoid any transfer step. To reach these objectives at a moderate cost, the growth of UTGF by chemical vapor deposition (CVD) and related processes using metallic catalyst appears promising technique. However, the elaborated graphene films using this technique contain undesirable impurities like hydrogen and impose other transfer steps, which can degrade the grapheme performance [7]. Another solution to avoid the transfer step is the formation of graphitic layers

from diamond-like carbon (DLC) films grown by pulsed laser deposition (PLD) at room temperature as well as by other PVD processes, followed by post-treatments. Under appropriate conditions, a tetrahedral amorphous carbon (ta-C) film is formed by PLD. These ta-C films exhibit many properties close to those of diamond, due to a high but tunable concentration of sp^3-hybridized carbon [8]. Moreover, they initially exhibit a sp^2-enriched surface [9, 10], that can be totally graphitized by subsequent thermal [11-14] or laser [15] treatments. A double process has been described in the literature including: 1) the clusterization into graphitic cycles of sp^2 single or olefinic chain sites initially embedded in a large network of sp^3 carbon at rather low temperatures (low activation energy) and 2) the direct transformation of sp^3 carbon to sp^2 carbon at higher temperatures (high activation energy). These post-treatments not only infer a drastic stress reduction, but also the films exhibit low surface conductivity. A derived elaboration process includes the incorporation of a catalytic transition metal like Ni, Pt… during or after the DLC deposition. It is presumed these metallic nanoparticles would act as catalytic centers accelerating the graphitization at lower temperatures. This effect has been early described in the literature with a conductivity variation of several orders of magnitude, but this result has thereafter no more received much attention [16]. The catalytic effect would indeed affect the graphitization process both on kinetic and thermodynamic viewpoints to elaborate high quality films, without structural or chemical modifications [14]. To the best of our knowledge, few studies have investigated the kinetics of graphitization of thin diamond-like carbon (DLC) films at a given temperature [17]. In this perspective, in this paper we report both thermal and kinetic studies of the graphitization of Ni/ta-C/quartz films to elaborate few graphitic layers on top of the ta-C film. Raman investigations, optical transmission and conductivity measurements have been carried out to investigate the optical and electrical properties of the elaborated films for eventual applications as transparent electrodes, biosensors and electrochemical cells [18, 19].

2. Materials and Methods

Samples were prepared by a triple step process. First carbon was deposited on quartz (double-face polished) by PLD at room temperature with a vacuum base higher than 10^{-3} Pa. A KrF laser source (248 nm wavelength, 30 ns pulse frequency) was used with a nuclear-grade graphite target (purity 5N) at a substrate-target distance of 5 cm. The laser fluence was within the range 4-6 J/cm^2, which corresponds to approximately 2×10^8 W/cm^2, a power density for

which we found a maximum of sp^3 carbon formation [20]. The deposited ta-C film thickness was around 15 nm. Further experimental details on the preparation, the determination of the sp^3/sp^2 ratio and the carbon density of the films are reported in references [20, 21]. Samples studied here have a density of about 3 g/cm^3 and 70% of sp^3 content.

Ni metal is subsequently deposited at room temperature by molecular beam epitaxy (MBE) on DLC/quartz samples at a minute amount of metal (around 0.15 nm of equivalent metal layer). The thickness of evaporated Ni was measured by Rutherford back scattering (RBS) as described in [22]. This is typically a deposition of less than one equivalent metallic monolayer, carried out 1) to avoid single layer formation and thus direct metallic surface conductivity and 2) to optimize the catalytic properties of small nanoparticles.

The samples Ni/ta-C/quartz were finally subjected to thermo-catalytic treatments in ultra-high vacuum (UHV) furnace (base pressure 10^{-4} Pa). The samples were taken out of the UHV chamber after each treatment. Then new measurements (Raman spectroscopy, UV-vis transmission, conductivity) were carried out before a new thermo-catalytic treatment was implemented. The samples Ni-DLC-3 samples were treated from 573K up to 873K by steps of 100K (Table 1). After setting the samples into the UHV furnace, a heating rate of 10K/min was applied up to the desired temperatures. After treatment was achieved, samples were cooled down in UHV without instructions. Samples DLC-1 and DLC-2 were similarly treated at 773K from a first treatment of 30 min up to a cumulative time of 3765 minutes with variable increasing time sequence. Besides, a reference sample (DLC-4), similar to DLC-3 sample but without catalyst was investigated at 773K for 60 min. Table 1 summarizes the properties of the samples used in this work. Sample Ni-DLC-1 and Ni-DLC-2 exhibit similar characteristics, except the thickness values, which are slightly different. As it has been reported that the microstructure of ta-C films changes along the axis normal to the surface [23], it is expected that the thickness could be a significant parameter in affecting the film performance. In addition, we check by ERDA that the samples are free from hydrogen impurities.

Sample	**Laser fluence (J/cm^2)**	**DLC thickness (nm)**	**Ni thickness (nm)**	**Annealing time (min) at 773K**	**Annealing temperature T at 60 min**
Ni-DLC-1	5	16	0.16	30-3765	773
Ni-DLC-2	5	13	0.13	30-3765	773
Ni-DLC-3	4.1	9.5	0.13	60	573-873K
DLC-4	5.6	9.5	-	60	873

Table 1: Main characteristics of the Ni/DLC/quartz samples

SEM images were obtained on a Zeiss GeminiSEM 500 working at 3 keV with secondary electrons emission and total yield detection modes, to contrast the topographic from the chemical information. Atomic force microscopy (AFM) both on a NT-MDT Stand Alone SMENA set-up is used in the resonant semicontact mode. Raman spectroscopy and mapping measurements have been carried out using a LabRam/Aramis Jobin/Yvon spectrometer with the green laser at 532 nm. The light was filtered to get a laser power of 1.5 mW on the sample to avoid damages in the carbon layer, using a 50 µm hole (confocal configuration), a monochromator of 2400 lines/mm and a magnitude lens of 100. Raman spectra were recorded in the 300-3000 cm^{-1} range. For Raman mapping, a set of 20×20 spectra distant each other by 0.5 µm was recorded. The spectra were then treated by removing the background and normalizing the signal to the intensity of the G signal. For some films, the light was focused either on the surface or at the interface with quartz. In the last case, the sample was turned with the light crossing the transparent quartz down to the interface. This was possible as the quartz samples were also polished on bottom face (RMS in the range 0.5-1.0 nm). Moreover, we tuned the intensity ratio of the G line with the Si line at 520 cm^{-1} to check the accuracy of the focalization. The conductivity measurements were performed using Hall effect technique (ECOPIA HMS-5000 set up) in the Van der Pauw configuration. Electric conductivity, in the planar orientation, as well as the nature, the mobility and the density of the carriers were determined. Knowing the thickness t (cm) of the conductive layer, the conductivity σ (S/cm) of the film can be expressed as:

$$\sigma = w / (t \times L \times R_s) \qquad (1)$$

where w and L are the width and the length of the sample, respectively, and R_s (Ω/□) denotes the sheet resistance.

The optical transmission of the films has been measured using a NIR Perkin ELMER spectrophotometer Lambda 19. The spectra were recorded from 250 to 850 nm, using a sweep rate of 120 nm/min. The slit width was fixed to 2 nm. Moreover, the recorded spectra were analyzed according to the approach described in [24], derived from Tauc's analysis, which can separately determine the nature of the optical transition and deduce the optical band gap E_g.

3. Results and discussion

A) Structural characterization

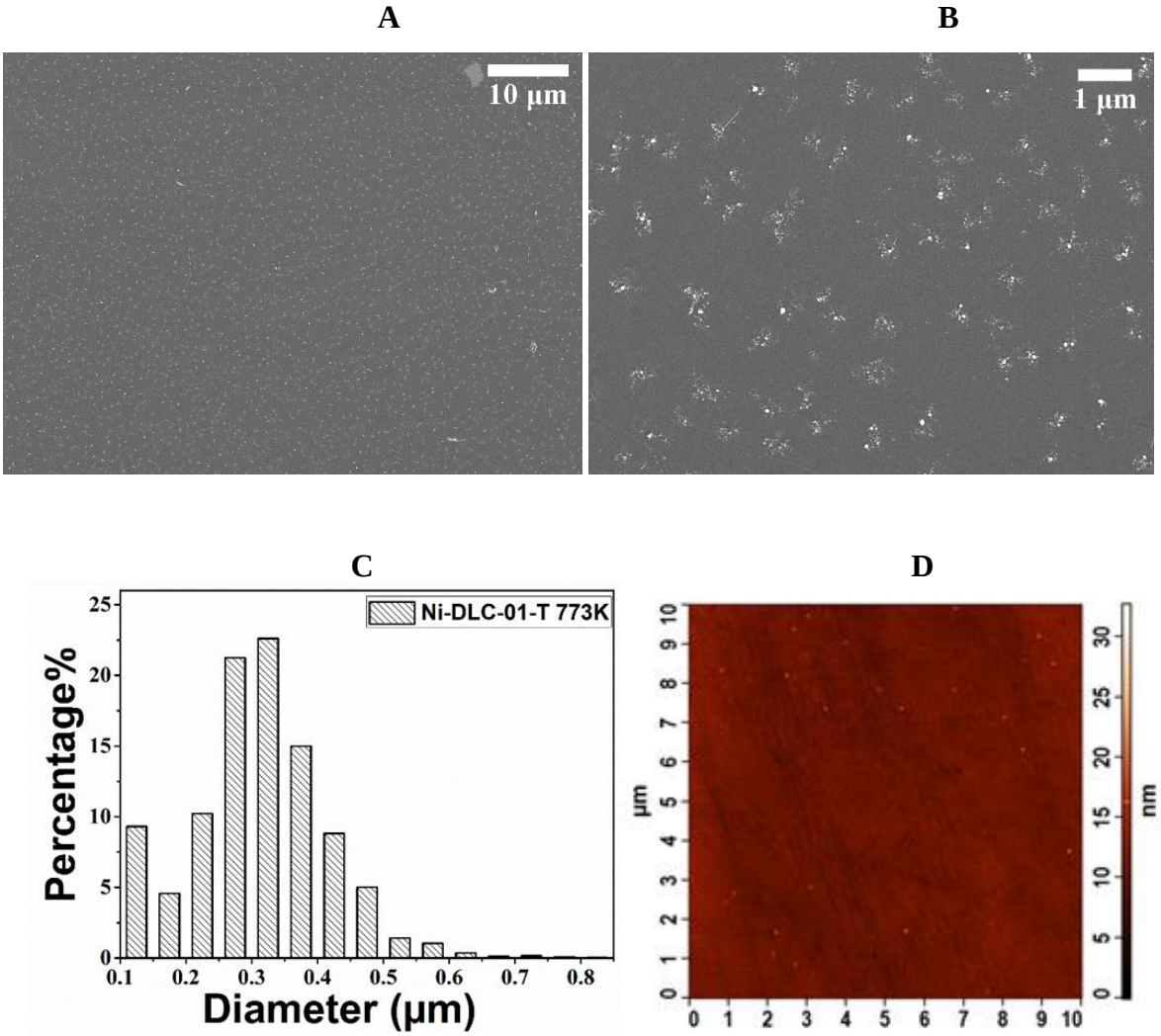

Fig.1 A) and B) SEM images of the Ni-DLC-1 sample after 3765 min of cumulative thermocatalytic treatment at two magnitudes; C) Histogram of the size distribution of set of nanoparticles displayed in Fig.1A on more than 2 500 nanoparticles using ImageJ software; D) AFM image of sample DLC-1 (without nickel).

A SEM image of the Ni-DLC-1 sample after 3765 min of cumulative thermocatalytic treatment at 773K is displayed at two magnitudes in Fig. 1A and B, respectively. The low magnitude spectrum shows a large and homogeneous spread of particles on the substrate. However, images recorded with a higher magnitude reveal that these spots are split into many single nanoparticles with a mean size of about 20-30 nm. This splitting can be the result of a possible carburization of the Ni particles. Ni in the presence of carbon can form a carbide phase Ni_3C which is thermodynamically stable within the temperature range 473-673K [25]. The decomposition of unstable Ni_3C particles above 673K might lead to such configuration

for the nanoparticles. The Ni nature of the nanoparticles is validated by energy-dispersive X-ray spectroscopy. The size distribution of the set of nanoparticles displayed in Fig. 1C and obtained over 2500 particles over a surface area of 208 μm^2 is randomly distributed with a maximum around 0.3 μm (Fig. 1C). The surface roughness was measured from AFM to 0.6 nm on sample DLC-1 (without nickel) (Fig. 1D).

B) Temperature treatment by Raman spectroscopy

We first investigated by Raman spectroscopy the effect of UHV thermal post-treatments. The sequence of Raman spectra (Ni-DLC-3 sample) are plotted on the surface and at the interface, respectively, as initially prepared and then after subsequent thermocatalytic treatments from 573 to 873K (Fig. 2A and B). From these figures, a broad complex band within the 1100-1650 cm^{-1} range characteristic of carbon contributions is recorded. These Raman spectra are roughly similar with previous reports on ta-C films prepared by PLD using the same nanosecond KrF source [9] or under similar conditions [26]. This broad band points out a D band centered around 1360 cm^{-1} and a G band centered at 1560-1590 cm^{-1}. The intense G band is due to the stretching 6E2g mode of sp^2-hybridized carbon whatever the nature (single, chain, cycle, …) of sp^2 carbon sites. By contrast, the D band is due to a multiphotonic process of sp^2 carbons and involves defects like edge sites of graphitic cycles. Thus, the ratio I_D/I_G of the intensities of these bands is a measurement of the cyclisation of the sp^2 carbon of nanometer size when starting from a highly defective carbon material like ta-C prepared at room temperature [27]. A careful analysis at the initial spectra focused on the surface shows that a D contribution is initially present at a low concentration. Thus, very small graphitic-like fragments are formed in the initial DLC structure. Nevertheless, it should be highlighted that the DLC structure consists in a sp^3-rich carbon network surrounding small sp^2-rich carbon fragments [8]. Therefore, other very weak contributions arise at around 1060 cm^{-1} (T mode), 1190 cm^{-1} (ν1) and 1480 cm^{-1}. (ν3) carbon vibration modes at the interface between the graphitic clusters in growth or in formation and the carbon sp3 network. The two latter lines are characteristic of disordered sp^3 hybridization state of carbon [8, 28], like sp3-hybridized carbons in close vicinity of the sp2 clusters. It is generally reported that the Raman ratio between sp3 and sp2 carbon is very weak [29], but in our case with a laser source at 2.33 eV and band gap around 1 eV, we may have some sp^3 carbon vibration modes.

Finally, the attribution of the T mode at 1060 cm^{-1} is more discussed, as being due either to carbyne chains or to diamond nanocrystalline form [28]. Besides, these lines are much more intense on the spectra recorded at the interface, which means that a higher level of sp^3

carbon is formed at the interface (Fig 2B). This suggests a gradient of sp^2/sp^3 carbon across the film, in agreement with the subplantation model of carbon DLC film growth [30-32]. By contrast the assignment of these lines to some Si-C bonds can be excluded [33].

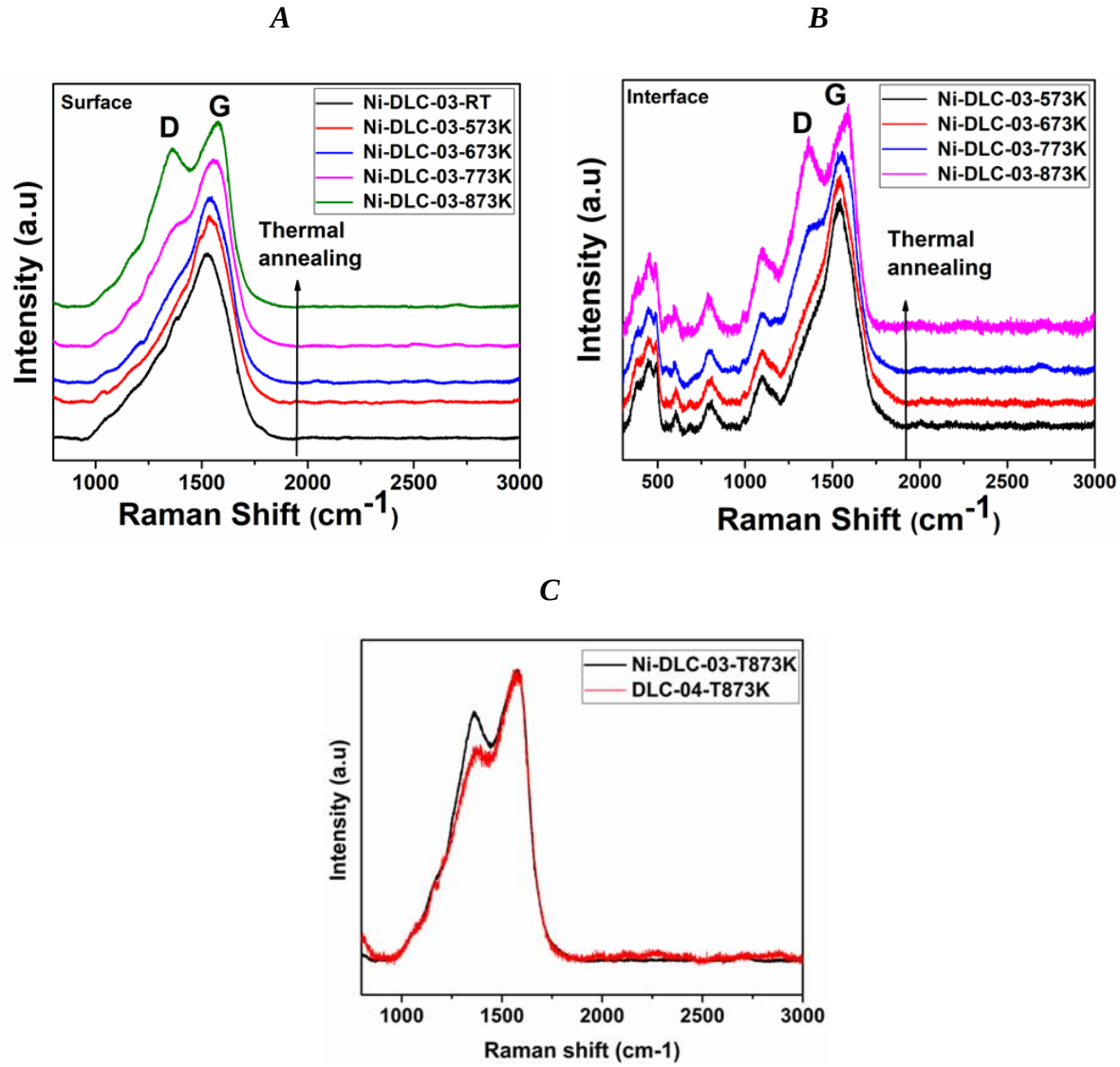

Figure 2: Raman spectra of Ni-DLC-3 sample after consecutive thermocatalytic treatments from 573 to 873K (100K stepwise, 60 min). A) surface and B) Interface analysis, respectively; C) Ni-DLC-3 (black) and DLC-4 samples (red) at 873K, 60 min.

Notable changes occur after successive thermocatalytic treatments from 573 to 873K. The intensity of the D band increases, the position of the G band shifts towards higher wavenumbers, from 1570 cm^{-1} to 1575-1580 cm^{-1}, and a narrowing of both D and G (from 170cm^{-1} to 130 cm^{-1}) bands occurs. By comparison, the ratio I_D/I_G is around 0.6 on the sample DLC-4 (without Ni)

instead of 0.75 on the sample Ni-DLC-3 after 60 min at 873K (Figure 2-C). This is an indication of the catalytic effect of the Ni particle for sp^2 carbon cyclization. These two effects are explained by the process of cyclization of carbon sp^2 fragments aggregating carbon sp^2 sites. Also, the arising at high temperature (T = 873K) of a weak 2D band at around 2700 cm^{-1} can be noticed (Fig.2 A). This 2D band is a multiphotonic process, and its occurrence can be considered as a signature of some weak organization of the graphitic fragments in the direction normal to the planar graphene plane. In contrast, sp^3 carbon bands do not change in intensity and remains weak. The lower wavenumber lines at around 500 and 800 cm^{-1} are due to Si-O and Si-Si vibrations and do not evaluate in intensity.

However, it is important to note that the DL films are not in an equilibrium state, and thus evolution of the carbon structure is not only temperature-dependent, but also may be time-dependent. This is why we performed a comprehensive kinetics study at a given temperature equals to 773K.

C) Kinetics of graphitization

1) Raman spectroscopy

The sequences of Raman spectra, recorded at both the surface and at the interface, are displayed as a function of the cumulative time of thermocatalytic treatment (from 30 to 3765 min) in Fig. 3A and B, respectively. From these figures, we observe a progressive increase of the D line compared to the G line. At the interface, we note also some weak but significant carbon sp^3 and T bands (with some dispersion of the intensities due to the error in the focalization at the interface), whereas the D and G bands characteristics of sp^2 carbon remains unchanged. We have calculated the ratio of intensities (surface areas) I_D/I_G according to a process analysis that has been described in more details in literature [21] and which is summarized here. The whole Raman lines in the range 1000-1650 cm^{-1} is fitted with five gaussian –shape contributions which are the G, D, ν3, ν1 and T lines around 1560-1590 cm^{-1}, 1360 cm^{-1}, 1470-1495 cm^{-1}, 1180 cm^{-1} and 1060 cm^{-1}, respectively. The baseline was first subtracted from Raman spectra before starting the analysis. Fig. 3 is an example of deconvolution of the Raman spectrum of the sample DLC-04 (773K-60 min). This analysis provides important information about each peak (FWHM, wavenumber, area and peak intensities). The intensity ratio of the two peaks D and G is used to evaluate the crystallite size of the sp2-hybridized carbons [27]. The surface I_D/I_G curves are plotted in Figure 3A for the Ni-DLC-1 and Ni-DLC-2 samples. For both samples, Ni-DLC-1 and Ni-DLC-2, this ratio starts with a slow raise, and then the increase becomes more pronounced above 200-300

minutes. The saturation apparently does not occur, even after near 4 000 minutes of thermal treatment. As these samples have rather similar characteristics, both curves give a good indication of the experimental dispersion of the results.

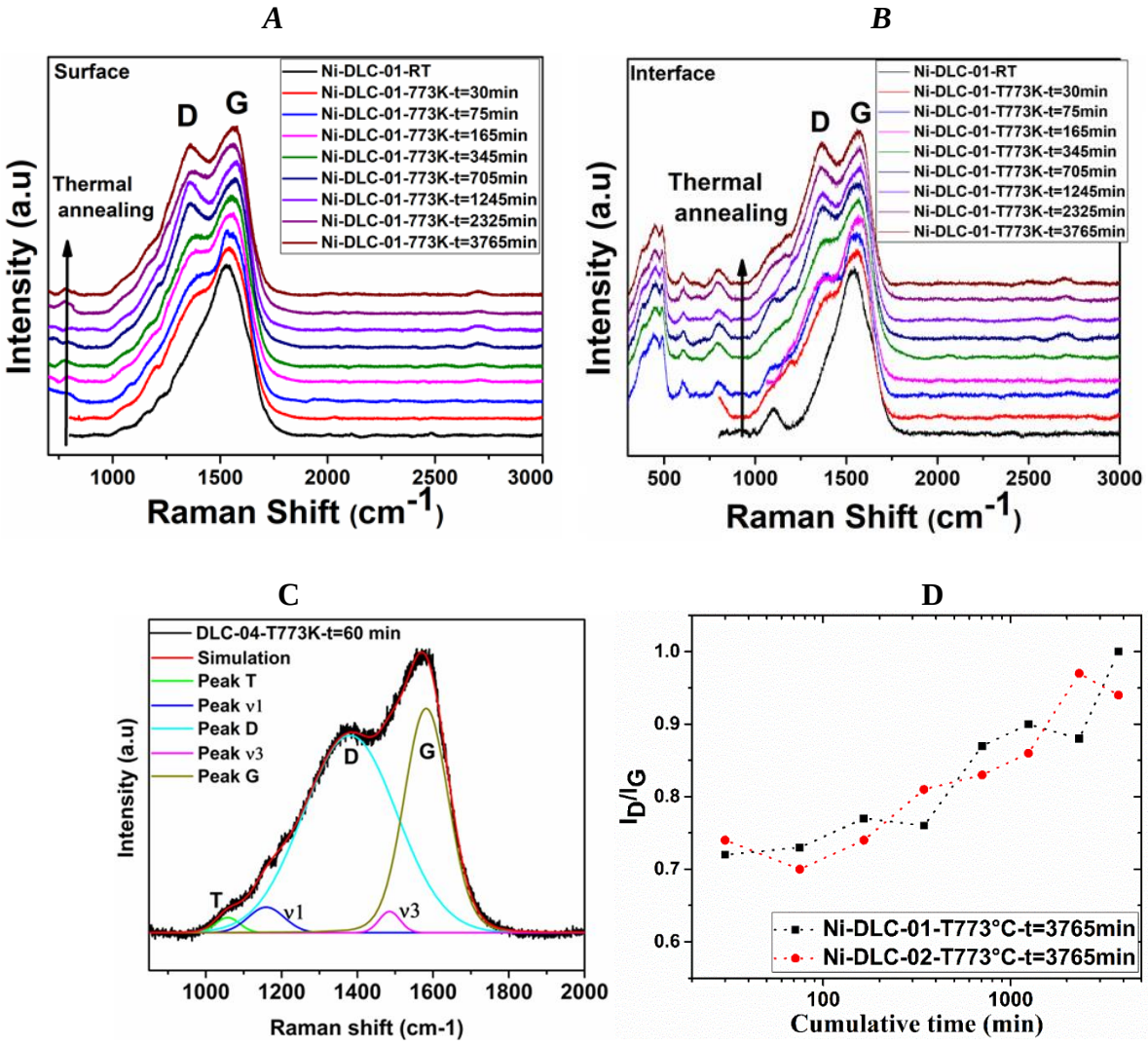

Fig 3 A) Sequence of Raman spectra as a function of cumulative thermocatalytic treatments at 773K in the range time 0-4000 minutes. Ni-DLC-1 sample. A) on the surface; B) at the interface; C) Fitting of DLC-4 at surface, 773K, 60 min and D) Variation of the Raman intensity (surface areas) ratio I_D/I_G as a function of cumulative thermocatalytic treatment at 773K. Ni-DLC-1 and Ni-DLC-2 samples.

If we consider that the variations of the D band are mainly due to the nucleation and growth of graphitic cycles, the increase of the I_D/I_G ratio is an indication of the formation and growth of graphitic cycles in the course of the thermocatalytic treatments. This formation of

graphitic cycles clearly takes a long time before completing stabilization and is not even achieved at 773K after 4 000 minutes of cumulative thermal treatments. Meanwhile, the G band remains stable around 1575 cm^{-1} and the FWHM of the G band decreases from 164 cm^{-1} to 137 cm^{-1}. It is expected however that the process involves not only the formation and growth of graphitic rings, but also ordering of the graphitic cycles and a reorientation of them in a direction parallel to the surface [28]. The occurrence of a weak 2D band at 2700 cm^{-1} above around 700 min of cumulative treatment, even if it remains invariably low, is an indication of a starting ordering of the graphitic layers.

2) Raman mapping

The Figs. 4A and B display the Raman surface mapping of the normalized intensities ratio I_D/I_G and I_{2D}/I_G obtained on the sample Ni-DLC-1 after thermocatalytic treatment of 3765 min at 773K, respectively, associated with the optical image on the same area (Fig. 4C). The two I_D/I_G images (Fig. 4A and D) are displayed with the same color amplitude of 0.3 (0.5-0.8 and 0.9-1.2 range, respectively, with mean values 0.65 and 0.95, in agreement with the I_D/I_G intensities reported in Fig. 3D of 0.75 and 0.95 at 180 min and 3765 minutes, respectively). Clearly, the last image displays bright areas contrasted with darker zones. The limited resolution of the camera however precludes to assign these areas to catalytic particles which are in the nanometer scale. The size of the catalytic domains (Fig 1B) is however of the same order of magnitude than the bright spots delivered by the optical image in Fig. 4C. Therefore, it is tempting to assign the small dark red domains with high I_D/I_G ratio values (1.15-1.20 in the intensity scale of Fig.4A) to the Ni large domains observed in Fig. 1. These areas can be assigned to preferential graphitic areas. In contrast, the areas with the lower I_D/I_G ratio values are considered as carbon sp^3-enriched domains. The mapping at 180 min exhibits much less contrast indicating that between 180 and 3765 min both nucleation and growth of domains with high I_D/I_G occur. Reversely, we fail to find a matching between the (I_{2D}/I_G) and the (I_D/I_G) mappings (Fig. 4A and 4B, respectively), or a matching between the (I_{2D}/I_G) mapping and the optical image (Fig 4B and 4C, respectively). The reason may be due to the very weak intensity of the 2D line, even after a long treatment at 773K. Moreover, it is likely that local conditions like roughness, orientation of the sp^2 cycles are more important at this level.

A **B**

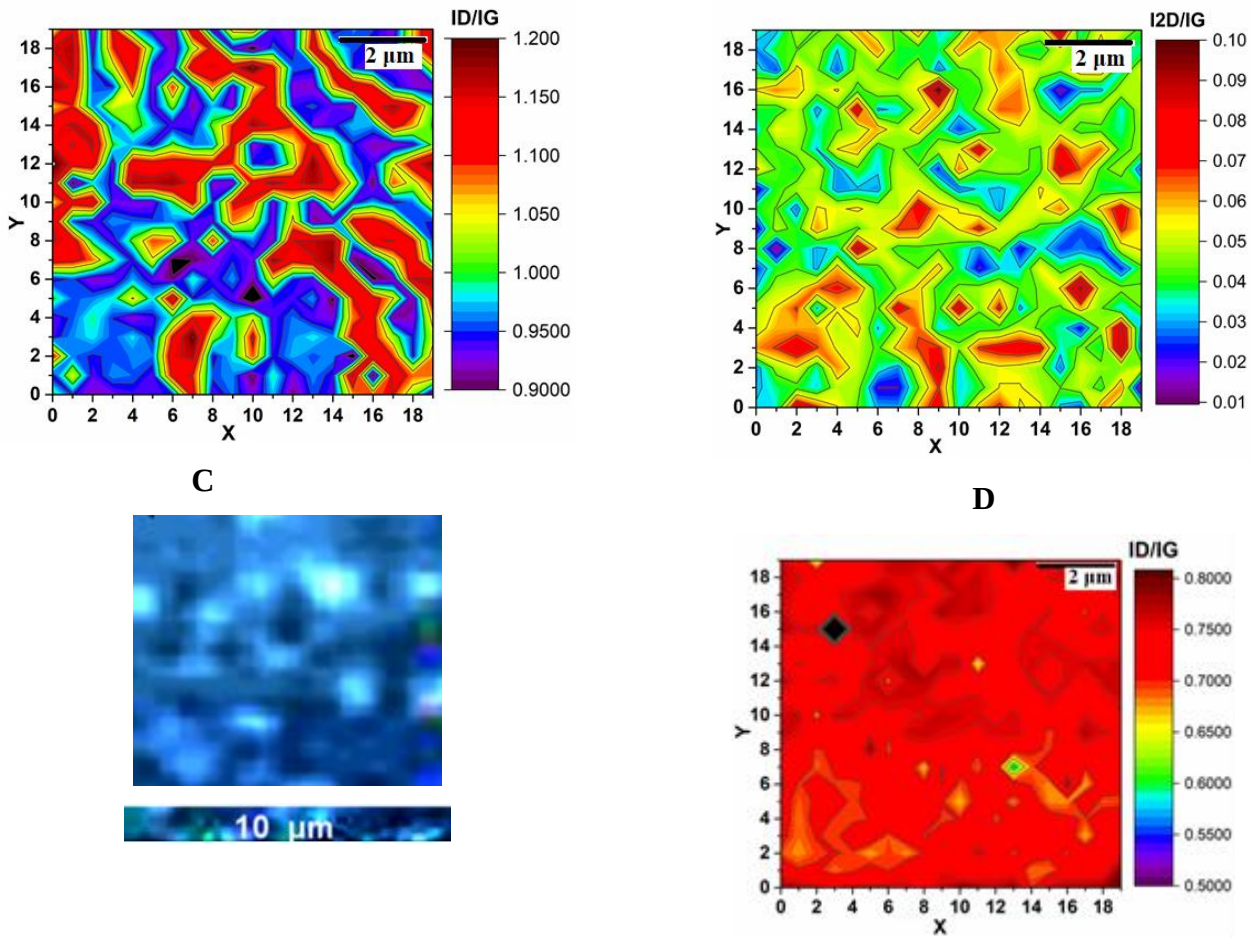

Fig. 4: A) and B): Raman images with a surface area of 100 µm² of the Ni-DLC-1 sample showing the ratio of normalized intensities (I_D / I_G) and (I_{2D} / I_G), respectively, after a thermocatalytic treatment of 3765 min at 773K. C) optical image of the same area. D) (I_D/ I_G) image of the same sample after thermocatalytic treatment of 180 min at 773K with the same amplitude (different area).

3) UV-vis transmission

The Fig 5A plots some optical transmission curves of the Ni-DLC-1 sample with successive thermocatalytic post-treatments at 773K in the UV-visible range 250-800 nm. The transmission of the quartz alone remains constant, at around 93%. In this figure, it is clearly shown the transmittance is decreased to 65% at 550 nm for Ni-DLC-1 sample. The influence of the metal deposition on the transmission spectrum of the untreated sample (not shown) is negligible. After a first treatment, at 773K for 30 min, the transmittance is slightly decreased to 55% at 550 nm. Then, some saturation is attended after approximately 1000 min (Fig. 5C in which the

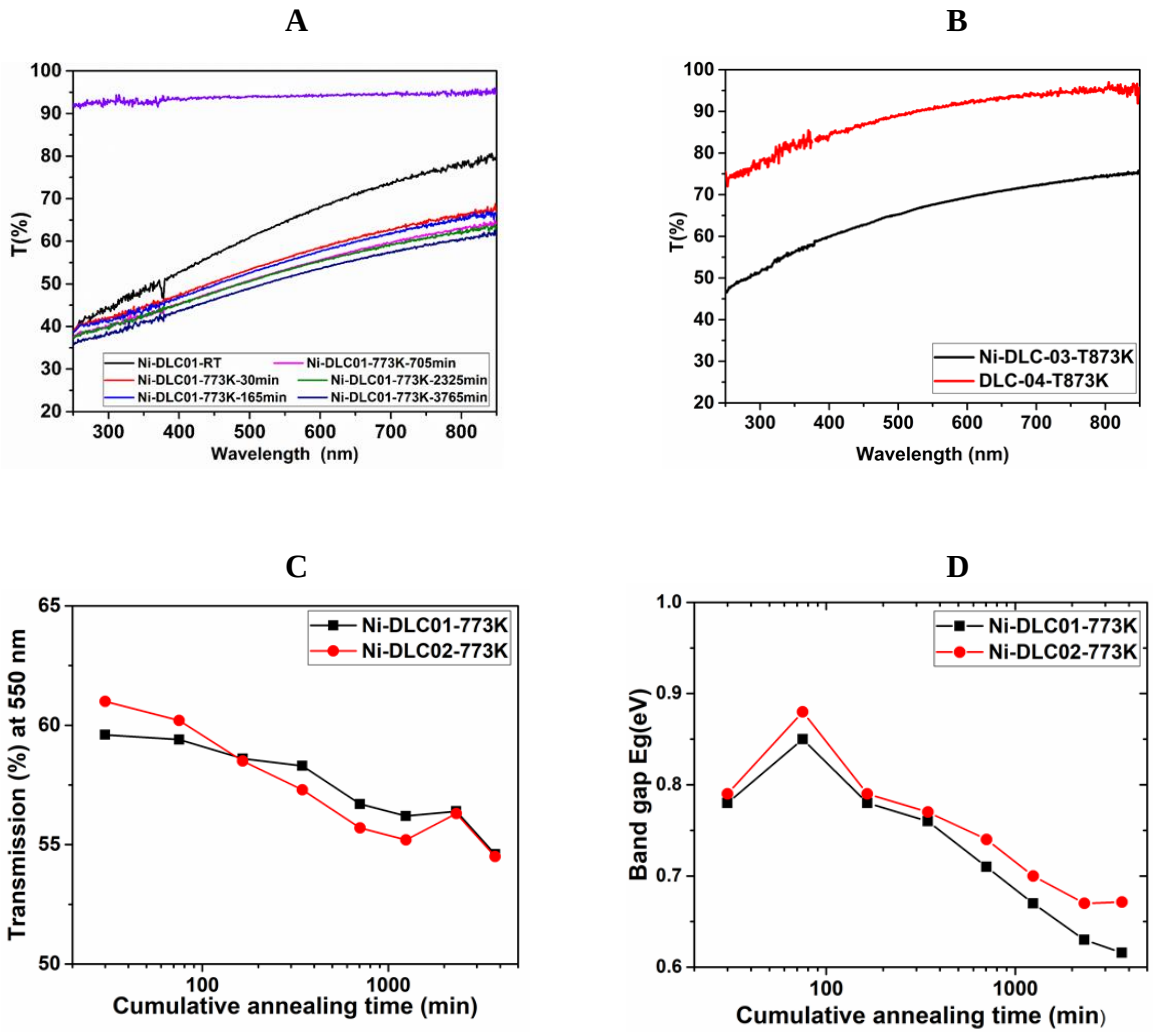

Fig.5: A) sequence of optical transmission on samples Ni-DLC-1 with cumulative thermocatalytic treatment. The transmission curve of the quartz is also reported. Scan rate of 120 nm/min; B) UV-Vis spectra of Ni-DLC3 (red) and DLC4 (black) at 873K, 60 min; C) Transmission (%) at 550 nm as a function of time (corrected from the quartz absorption); D) Band gap as a function of time (extracted from the transmission curves according to [24].

transmissions at 550 nm are corrected for the quartz absorption). These results are in good agreement with the progressive formation of graphitic aromatic clusters. However, a close inspection in the near-UV range reveals some slight changes in the transmittance behavior. Fig 5D plots the variation of optical band gap E_g as function of time extracted according to [24]. E_g is initially measured on DLC-01 and DLC-02 samples at 1.1 eV. It drops to 0.95 eV with deposition of nickel. Starting the thermal treatment at 773K, it drops again to slightly less than 0.8 eV. It is shown in Fig.5D that the optical band gap increases first with time to reach a

maximum value of 0.85-088 eV for an annealing time equals to 60 min. After 60 min, the optical band gap is decreased to near 06-065 eV with some trend to saturation. This signifies that the cumulative annealing time has a significant impact on the DLC film electrical behavior.

We finally compare the samples Ni-DLC-3 and DLC-4 (without Ni) of same thickness and both treated 60 min at 873K (Fig. 5B). The sample DLC-4 exhibits a transmission of around 90% at 550 nm, much higher than the transmission on Ni-DLC-3 sample around 65%. This is a clear evidence of the catalytic behavior of Ni which accelerates the formation of aromatic domains, highly absorbing the light.

4) Transport measurements

We have first checked that the untreated Ni-DLC-01 and Ni-DLC-02 samples exhibit no conductivity within the detection limits (less than 10^{-3} S/cm). The same behavior is observed for the DLC-4 sample without catalyst annealed at 773K for 60 min.

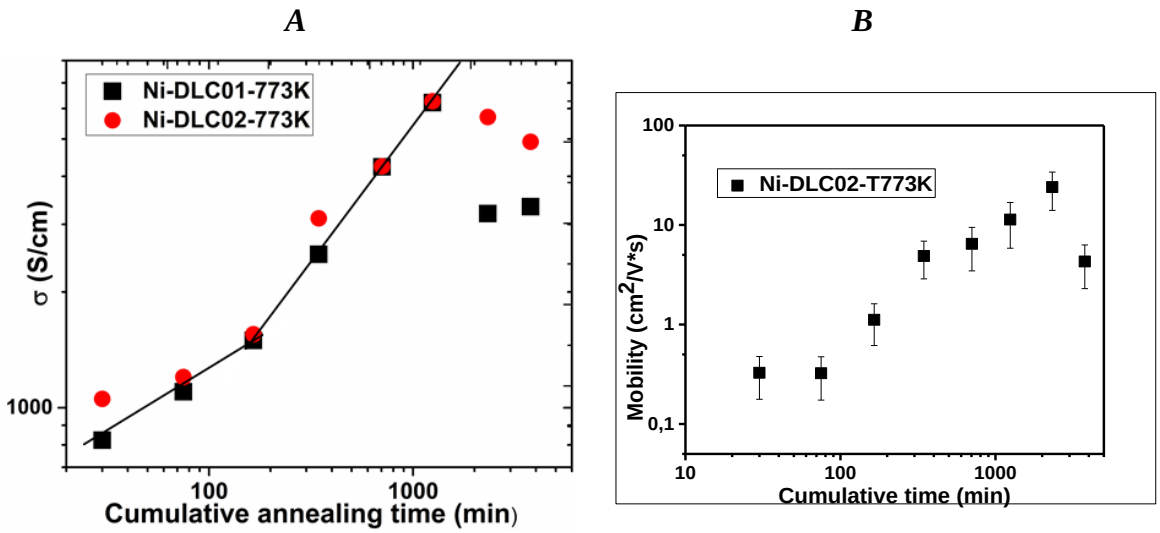

Fig. 6: Logarithmic plots of A) Conductivity (S/cm) measured in the Van der Pauw configuration (the linear correlations display the two first regimes as discussed in the text); B) Carrier mobility as a function of the cumulative annealing time (Ni-DLC-2 sample).

Fig 6A illustrates the variation of the electrical conductivity, σ, versus the cumulative annealing time. From this figure, it is clearly shown that the samples Ni-DLC-1 and Ni-DLC-2 exhibit high conductivity values in the 10^3-10^4 S/cm range. The conductivity behavior shows three power regimes in a logarithmic scale. The first one, up to 200 min, displays a small increase with a linear slope of 0.32, the second one occurs in the range 200-1500 min with a

steeper increase (linear slope of 0.7) and finally a saturation or even a slight decrease is observed above 1000 min. The overall increase is larger than one order of magnitude (Fig. 6A), from initially around 8.10^2 S/cm to 7.10^3 S/cm after 1245 min of cumulative thermocatalytic treatment. The two samples yield very similar conductivities, except for the third regime. The main conclusion is that the transport conductivity of Ni-DLC samples is never stabilized at 773K of annealing temperature over a large range time.

We compared the conductivities of Ni-DLC-3 and DLC-4 samples treated under the same conditions (873K, 30 min). We find $1.9\ 10^3$ S/cm for the metal-loaded sample and we do not observe any conductivity on the unloaded sample. The catalytic effect of the metal on conductivity is clearly observed.

The mobilities of the carriers are reported in Fig. 6B for Ni-DLC-2 sample. The Hall effect measurements indicate that conductivity of thin layers graphite was both due to positive (holes) and negative charge carriers (electrons). This affects the determination of the Hall constant of the carrier mobility and of the carrier concentration.

The Hall constant R_H is then expressed as

$$R_H = (1/e)\times(p - n\times b^2) / (p + (n\times b))^2 \qquad (2)$$

where p and n are the positive and negative carrier concentrations, respectively, and $b = \mu_e/\mu_h$ is the ratio of the mobility values. The total density of charge carriers n+p can then be expressed as:

$$n+p = (1+R) \times (1-R\times b^2) / e\times R_H \times (1+R\times b)^2 \qquad (3)$$

The electron and hole mobilities μ_e and μ_h, respectively, defined as $\sigma = (\mu_e\times e\times n + \mu_h\times e\times p)$, can be expressed as:

$$\mu_e = R_H \times b\times\sigma / (1-R\times b^2) \qquad (4)$$

and

$$\mu_h = \mu_e / b = R_H\times\sigma / (1-R\times b^2) \qquad (5)$$

where R = n/p is the ratio of charge densities. Neglecting again the contribution of impurities, we take this ratio as R = 1.33 obtained on pyrolytic graphite [34]. To support this

assumption, it has been checked by a statistical analysis (more than 100 independent Hall measurements) that the ratio of major n type over p type conductivity is 1.24. Fig. 6B reveals that the electron mobility increases with time to reach a maximum mobility value of 20 $cm^2/(V\times s)$ for a thermocatalytic time equals to 2000 min. The carrier density given by equation (3) is quoted to around 10^{20}-10^{21} cm^{-3}. It must be noted that the transport properties obtained, with mobility of around 20 $cm^2/V.s$ at the best, are quite comparable with a recent publication on ta-C:H samples annealed at higher temperatures [35].

Discussion

It is worthy to mention that the kinetics of surface conductivity is rather complex and its interpretation needs further investigation. However, it is possible to rely such behavior with the Raman analysis.

The relation between the conductivity and the nanostructure has been often studied in ta-C films, but only the thermal effect has been investigated on ta-C [17, 36, 37] and ta-C-H films [38]. Two processes occur that contributes in improving the conductivity with time or temperature: 1) clustering of the sp^2 phase into sp^2 cyclic domains and 2) carbon sp^3 to carbon sp^2 conversion. However, owing to high activation energy we can rule out this last process that occurs only at high temperatures. Moreover, the sp^2 cluster orientation is also important in the surface conductivity, with an optimum configuration for surface conductivity when the cluster domains are oriented parallel to the surface. At room temperature, transport in ta-C films can be described by hopping between near neighbor sp^2 clusters and the conductivity σ. The latter is expressed as [36, 37]:

$$\sigma = K\times(d^2/T) \times \exp\{-[E / (k\times T)] - (2\times d)/a]\} \qquad (6)$$

where *a* is the localization radius of the conducting states, d is the distance between the near neighbor sp^2 clusters, E expresses the activation energy of the transport process and K is a constant. Assuming a random and homogeneous distribution of graphitic spherical clusters, the localization radius *a* can be assigned to the cluster radius. The hopping distance d can be expressed as $d = D - 2a$, where D is the mean distance between two near-neighbor sp^2 clusters. Then D can be expressed as a function of the cluster density N as $D = k / N^{1/2}$, where N represents the cluster density. Thus, the hopping distance d can be expressed as a function of the cluster density N and the cluster mean size as:

$$d = (k / N^{1/2}) - 2a \qquad (7)$$

at a fixed temperature and from expressions (6) and (7), the conductivity can be given by:

$$\sigma = K'(T) \times [(k / N^{1/2}) - 2a]^2 \times \exp\{- [2 \times k / (a \times N^{1/2})] \qquad (8)$$

where K'(T) is a constant that involves all the temperature-dependent parameters. In the absence of any more data about the independent time variations of the localization radius a(t) and the cluster density N(t), it is difficult to go further in the analysis without supplementary assumptions. However, the localization radius is correlated to the cluster size L_a in a hopping transport model as:

$$a = C \times La / [E_\pi(L_a) - E_\sigma]^{1/2} \qquad (9)$$

where $E_\pi(L_a)$ and E_σ are the electronic gaps between π-π^* and σ-σ^* states, respectively. $E_\pi(L_a)$ is strictly depending on the cluster size as reported by Robertson [39]. For large clusters however, like here as ascertained by large Raman I_D/I_G ratio, $E_\pi(L_a)$ is constant, so $a \approx C_1 \times L_a$ with $C_1 = C / [E_\pi - E_\sigma]^{1/2}$. In the phase of graphitic clusters growth with increasing I_D/I_G, $I_D/I_G \propto L_a^2$ [27]. Moreover, we can assume that the density N(t) is rapidly constant as the metal particle acts as a nucleation center for graphitic clusters, then $N(t) \approx N_0$. Then equation {8} reduces to:

$$\text{Ln } \sigma = C(T) - (D / (I_D/I_G)^{1/2}) \qquad (10)$$

A plot of Ln σ = versus $(I_D/I_G)^{-1/2}$ is displayed in Figure 7 for both samples Ni-DLC-1 and Ni-DLC 2 samples. It shows a reasonable agreement with a negative linear slope of -1/2, considering the error on I_D/I_G.

Another explanation can be found in close insight on the variations of the Raman ratio I_D/I_G with time. This ratio is expected to be dependent on both the density and on the size of the cluster radius, and clearly supports the increase of the conductivity with time. Moreover, the power laws with time distinguish two regimes. We propose that the first regime is a nucleation kinetics domain, where the conductivity is mainly governed by the variations of $N^{1/2}$, whereas

the second regime is a growth kinetics regime which is mainly governed by the variations of the mean size *a*. This could be related to the slope ratio between the first and the second regime around 0.32 / 0.7 ≈ 0.46, not far from ½ as expected from equation (8). Moreover, the improvement of the conductivity at a given temperature may be also the result of a reorientation of the sp^2 clusters from the normal direction to the surface to an orientation parallel to the substrate. In the PLD process under our conditions it is believed that carbon ions impinge the surface with kinetic energy around 100 eV or more. Within these kinetic energies sp^2 carbon may be formed with a preferential orientation along the pathway of carbon ions inside the ta-C film, thus rather perpendicular to the surface. This has been shown for example for the formation of graphitic clusters normal to the surface during the diamond nucleation assisted by carbon ion bombardment [40]. It is expected that the graphitic clusters will tend to reorient themselves with time or temperature in the direction parallel to the surface or the interface with substrate to minimize the bi-axial stress of the graphitic cluster sheets.

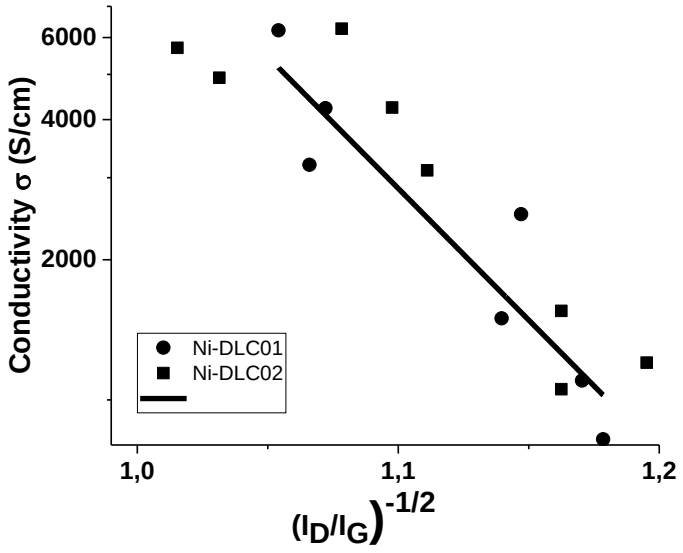

Fig. 7: Correlation between the conductivity variation and the Raman I_D/I_G ratio according to the equation (10).

Therefore, the improvement of the conductivity at a given temperature may be also the result of a reorientation of the sp^2 clusters from a direction normal to the surface to an orientation parallel to the substrate. This is supported by the literature report where conductivities were recorded in both direction, perpendicular and parallel directions to the surface as a function of thermal treatment. A cross is clearly observed between two

measurements [37]. This process is expected to be a slow process as it involves the movement of the carbon atoms of the graphitic cluster. Finally, the last regime is a saturation/degradation of the conductivity. It is proposed that in this regime the density and/or the size of the graphitic clusters become so high that their coalescence starts.

4. Conclusions

In this work, we have studied the kinetics of graphitization at 773K of thin diamond-like carbon (DLC) films coated with Ni metallic nanoparticles. DLC films are deposited at room temperature by pulse laser deposition (PLD) on a transparent quartz substrate. Moreover, a Ni metal (less than one equivalent monolayer) is deposited on the surface of DLC using molecular beam epitaxy technique at room temperature in order to create Ni nanoparticles. Ultra-high vacuum annealing treatments (range 573-873K with 60 min) show a transformation of carbon sp^2 single or chain sites into cyclic aromatic domains which is probed by the Raman I_D/I_G ratio. Studied for the first time to our knowledge, a comprehensive kinetic study of thermocatalytic treatments on Ni-DLC samples in the range 30-3760 min at 773K shows a continuous process of sp^2 clusters formation and growth using Raman spectroscopy, optical transmission and electrical conductivity measurements. The kinetic behavior is analyzed in terms of nucleation and growth of graphitic sp^2 clusters, probably encompassed by a long-range kinetics of reorientation of the graphene layers of the graphitic clusters moving from normal to parallel direction to the surface and the interface. A correlation is found between the Raman I_D/I_G ratio and the conductivity in agreement with the nucleation and growth of graphitic clusters. Further studies are however required to monitor independently the kinetic of graphitic cluster formation, growth, orientation and coalescence. High surface electrical conductivities are reached accordingly, at more than 6×10^3 S/cm, with carrier mobility equals to 20 $V/cm^2\times s$ and a high density of carriers which are almost equally positive and negative. These characteristics make the elaborated DLC film potentially suitable for developing new high performance conductive electrodes and optoelectronic sensors.

Acknowledgements: The authors would like to thank: T. Fix (Hall measurements), F. Stock (optical transmission analysis); N. Roques, D. Muller (NRA and RBS) at ICube/MaCEPV, Strasbourg; J. Faerber (SEM) and J. Arabski (MBE) at IPCMS, Strasbourg, are acknowledged for their contributions. Part of this research was supported by Exceptional National Program (178 / P.N.E), funded by the Ministry of Higher Education and Scientific Research of Algeria, which is thanked for this fellowship.

REFERENCES

[1] Avouris P. and Dimitrakopoulos C., "Graphene: Synthesis and Applications"; *Mater. Today*, **15** (2012) 86-97.

[2] Castro Neto A.H., Peres N.M.R., Guinea F., Novoselov K.S. and Geim A.K., "The electronic properties of graphene"; *Review of Modern Physics*, **81** (2009) 109-162

[3] Jang W.Y., Chen Z., Bao W.Z., Lau Z.N. and Dames C., "Thickness-Dependent Thermal Conductivity of Encased Graphene and Ultrathin Graphite"; *Nano Letters*, **10** (2010) 3909–3913

[4] Lee C.G., Wei X.D., Kysar J.W. and Home J., "Measurement of the Elastic Properties and Intrinsic Strength of Monolayer Graphene"; *Science*, **321** (2008) 385-388

[5] Blake P., Hill E.W., Castro Neto A.H., Novoselov K.S., Jiang D., Yang R., Booth T.J. and Geim A.K., "Making graphene visible"; *Applied Physics Letters*, **91** (2007) 063124/1-3.

[6] Ferrari A.C., Bonaccorso F., Fal'ko V., Novoselov K.S., Roche S., Bøggild P., Borini S., Koppens F. H. L., Palermo V., Pugno N., Garrido J.A., Sordan R., Bianco A., Ballerini L., Prato M., Lidorikis E., Kivioja J., Marinelli C., Ryhänen T., Morpurgo A., Coleman J.N., Nicolosi V., Colombo L., Fert A., Garcia-Hernandez M., Bachtold A., Schneider G.F., Guinea F., Dekker C., Barbone M., Sun Z., Galiotis C., Grigorenko A.N., Konstantatos G., Kis A., Katsnelson M., Vandersypen S., Loiseau A., Morandi V., Neumaier D., Treossi E., Pellegrini V., Polini M., Tredicucci A., Williams G.M., Hong B.H., Ahn J.H., Kim J.M., Zirath H., Van Wees B.J., Van der Zant H., Occhipinti L., Di Matteo A., Kinloch I.A., Seyller T., Quesnel E., Feng X.L., Teo K., Rupesinghe N., Hakonen P., Neil S.R.T., Tannock Q., Löfwander T. and Kinaret J., "Science and technology roadmap for graphene, related to-dimensional crystals, and hybrid systems", *Nanoscale* **7** (2015) 4598-4810

[7] Reina A., Jia X.T., Ho J., Nezich D., Son H.B., Bulovic V., Dresselhaus M.S. and Kong J., "Large Area, Few-Layer Graphene Films on Arbitrary Substrates by Chemical Vapor Deposition"; *Nano Letters*, **9** (2009) 30-35

[8] Robertson J., "Diamond-like amorphous carbon"; *Materials Science and Engineering*, **R37** (2002) 129-281

[9] Fallon M.J., Veerasamy V.S., Davis C.A., Robertson J., Amaratunga G.A.J., Milne W.I. and Koskinen J., "Properties of filtered-ion-beam-deposited diamondlike carbon as a function of ion energy"; *Phys. Rev. B*, **48**, (1993), 4777-4782

[10] Rey S., Antoni F., Prevôt B., Fogarassy E., Arnault J.C., Hommet J., Le Normand F. and Boher P., "Thermal stability of amorphous carbon films deposited by pulsed laser ablation"; *Applied Physics A*, **71** (2000) 433-439

[11] Orwa J.O., Andrienko I., Peng J.L., Prawer S., Zhang Y.B., and Lau S.P., "Thermally-induced sp^2 clustering in tetrahedral amorphous carbon (ta-C) films"; *Journal Applied Physics*, **96** (2004) 6286-6297

[12] Chhowalla M., Ferrari A.C., Robertson J., Amaratunga G.A.J., "Evolution of sp2 bonding with deposition temperature in tetrahedral amorphous carbon studied by Raman spectroscopy"; *Applied Physics Letters*, **76** (2000) 1419-1421

[13] Ferrari A.C., Stolojan V., Morrison N.A., Hart A., Kleinsorge B. and Robertson J., "Stress reduction and bond stability during thermal annealing of tetrahedral amorphous carbon"; *Journal of Applied Physics*, **85** (1999) 7191-7197

[14] Sullivan J.P., Friedmann T.A. and Baca A.G., "Stress relaxation and thermal evolution of film properties in amorphous carbon"; *Journal of Electronic Materials*, **26** (1997) 1021-1029

[15] Jung H.S., Park H.H., Pang S.S. and Lee S.Y., "The investigation of thermal effect on the properties of pulsed laser deposited diamond-like carbon films"; *Thin Solid Films*, **332** (1998) 103-108

[16] Dimigen H., Hubsch H. and Memming R., "Tribological and electrical properties of metal-containing hydrogenated carbon films"; *Applied Physics Letters*; **50** (1987) 1056-1058

[17] Sullivan J.P., Friedmann T.A., Dunn R.G., Stechel E.B., Schultz P.A., Siegal M.P. and Miessert N., "The electronic transport mechanism in amorphous tetrahedrally-coordinated carbon films"; *Proceedings Materials Society Symposia***; 498** (1999) 97-102

[18] Tamulevičius S., Meškinis S., Tamulevičius T. and Rubahn H.G., "Diamond like carbon nanocomposites with embedded metallic nanoparticles"; *Reports on Progress in Physics***; 81** (2018) 024501/1-31

[19] Bewilogua K. and Hofmann D., "History of diamond-like films: from first experiments to worldwide applications"; *Surface Coatings Technology***, 242** (2014) 214-225

[20] Stock F., Antoni F., Le Normand F., Muller D., Abdesselam M., Boubiche N. and Komissarov I., "Diamond-Like Carbon layers obtained by Pulsed Laser Deposition in different conditions for conductive electrodes application"; *Applied Physics A: Materials Science & Processing;* **123** (2017) 590-595

[21] Boubiche N., Aweke F., Hulik J., Luo W., Abdesslam M., Zafeiratos S.; Djeffal F., Le Normand F., "Ultrathin DLC films coated with transition metals and its transformation into graphitic films by thermal or thermocatalytic treatments »; *in preparation*

[22] Bouanis F.Z., Florea I., Bouanis M., Nyassi A., Muller D., Le Normand F., Pribat D., "Diameter-controlled growth of SWCNTs using Ru as catalyst precursors coupled with hydrogen treatment", *Chemical Engineering Journal*, **332** (2017) 92-101

[23] Siegal M.P., Tallant D.R., Provencio P.N., Simpson R.L., Kleinsorge B., Milne W.I., "Bonding topologies in diamondlike amorphous carbon films", *Applied Physics Letters* **76** (2000) 2047-2049

[24] Changshi L. and Feng L. "Optical gap determination"; *Optics Communications***; 285** (2012) 2868-2873

[25] Sinharoy S., Smith M.A. and Levenson L.L., "The formation and decomposition of nickel carbide in evaporated nickel films on graphite"; *Thin Solid Films* **53** (1978) 31-36

[26] Kalish R., Lifshitz Y., Nugent K. and Prawer S., "Thermal stability and relaxation in diamond-like-carbon. A Raman study of films with different sp^2/sp^3 fractions (ta-C to a-C)"; *Appl. Phys. Letters*, **74** (1999) 2936-2398

[27] Ferrari A.C. and Robertson J., "Interpretation of Raman spectra of disordered and amorphous carbon"; *Phys. Rev. B*, **61** (2000) 14095-14107

[28] Chu P.K. and Li L.H., "Characterization of amorphous and nanocrystalline carbon films"; *Materials Chemistry and Physics*, **96** (2006) 253-277

[29] Wada N. and Solin S.A. "Raman efficiency measurements of graphite"; *Physica B*, **105** (1981) 353-356.

[30] Mac Kenzie D.R., Muller D. and Pailthorpe B.A., "Compressive-stress-induced formation of thin-film tetrahedral amorphous carbon"; *Phys Review Letters*, **67** (1991) 773-776

[31] Siegal M.P., Tallant D.R., Provencio P.N., Overmyer D.L., Simpson R.L., Martinez-Miranda L.J., "Ultrahard carbon nanocomposite films"; *Applied Physics Letters***; 76** (2000) 3052-3054

[32] Siegal M.P., Barbour J.C., Tallant D.R., Provencio P.N., and Friedmann T.A. "Amorphous-tetrahedral diamondlike carbon layered structures resulting from film growth energetics"; *Applied Physics Letters,* **73** (1998), 759-761

[33] Inoue Y., Nakashima S. and Mitsuishi A., “Raman spectra of amorphous SiC”; *Solid State Communications,* **48** (1983) 1071-1075[34] Klein C.A. and Straub W.D., “Carrier densities and mobilities in pyrolytic graphite”, *Physical Review,* **123** (1961) 1581-1583

[34] Klein C.A. and Straub W.D., “Carrier densities and mobilities in pyrolytic graphite”, *Physical Review,* **123** (1961) 1581-1583

[35] Zhai Z.H., Shen H.L., Chen J.Y., Li X.M. and Jiang Y., “Evolution of structural and electrical properties of carbon films from amorphous carbon to nanocrystalline graphene on quartz glass by HFCVD”; *ACS Applied Materials and Interfaces,* **10** (2018) 17427-17436

[36] Ilie A., “Electronic transport, photoconductivity and photoluminescence in amorphous carbon”; *Diamond Related Materials,* **10** (2001) 207-215

[37] Ilie A., Ferrari A.C., Yagi T., Rodil S.E., Robertson J., Barborini E. and Milani P. « Role of sp^2 phase in field emission from nanostructured carbons”; *Journal of Applied Physics,* **90** (2001) 2024-2032.

[38] Dasgupta D., Demichelis F. and Tagliaferro A., “Electrical conductivity of amorphous carbon and hydrogenated amorphous carbon”; *Philosophical Magazine B,* **63** (1991) 1255-1266

[39] Robertson J. and O’Reilly E.P., “Electronic and atomic structure of amorphous carbon”; *Phys. Rev. B.,* **35** (1987) 2946-2957.

[40] Lifshitz Y., Lee S.T., Meng X.M., Akhveldiany R. and Hoffman A., “Visualization of Diamond Nucleation and Growth from Energetic Species”; *Phys. Rev. Letters,* **93** (2004), 056101.